Environmental Science Nano

COMMENT

Cite this: *Environ. Sci.: Nano*, 2018, 5, 2198

Comment on "Crystal growth and aggregation in suspensions of δ-MnO_2 nanoparticles: implications for surface reactivity" by F. F. Marafatto, B. Lanson and J. Peña, *Environ. Sci.: Nano*, 2018, 5, 497†

Alain Manceau

Received 29th January 2018,
Accepted 16th April 2018

DOI: 10.1039/c8en00126j

rsc.li/es-nano

Here, it is shown that X-ray diffraction is sensitive to the lognormal distribution of the δ-MnO_2 crystallite size and to the strain gradient across the nanosheet. Rigorous modeling of the two effects, which were overlooked by Marafatto *et al.* (*Environ. Sci.: Nano*, DOI 10.1039/c7en00817a), is essential to understand the influence of non-uniform microstructures on the physicochemical properties and surface reactivity of nanoparticulate δ-MnO_2.

Marafatto *et al.*[1] used laboratory powder X-ray diffraction (XRD) to determine the layer and interlayer structures and lateral size of δ-MnO_2 nanosheets synthesized at pH 6, 8 and 11. The structures were obtained by fitting *full* XRD patterns in the $30° < 2\theta(\text{CuK}\alpha) < 75°$ interval, which includes the 20,11 and 02,31 *hk* scattering bands. The lateral size was estimated from the diameter of the coherent scattering domains (CSDs) deduced from the modeling of the 20,11 band. The CSD values were observed to decrease from 7.2 ± 0.5 nm to 2.8 ± 0.5 nm when the suspension pH was increased from 6 to 11. This trend was confirmed by measuring the full width at half-maximum (FWHM) of the 02,31 band with a synchrotron X-ray source. However, the variation of the crystallite size with pH was extremely different when obtained by calculation from the fit of the 20,11 band and by experiment from the measurement of the 02,31 width. This difference leads to the two questions:

1 – Why are the results obtained from the analysis of the 20,11 and 02,31 reflections inconsistent? It is proposed that the change with pH of the lognormal distribution of the crystallite size[2] was overlooked in the fit of the 20,11 profile.

2 – How were the *full* XRD patterns fit without modeling the non-uniform strain of the δ-MnO_2 crystallites resulting from the bending of the nanosheets?[2] A full-pattern fit can be obtained by separately fitting and then joining the 20,11 and 02,31 reflection lines without considering the non-uniform strain. However, the non-uniform strain would have significant bearing on the macroscopic physicochemical properties and surface reactivity of these δ-MnO_2 crystallites, and therefore must be considered.

Univ. Grenoble Alpes, CNRS, ISTerre, F-38000 Grenoble, France.
E-mail: alain.manceau@univ-grenoble-alpes.fr

† Electronic supplementary information (ESI) available. See DOI: 10.1039/c8en00126j

Correlation between the arithmetic mean and standard deviation of the crystallite size distribution

As shown in Fig. 1A, varying the CSD dimension modifies the width of both the 20,11 and 02,31 reflections.[3] Thus, as a first approximation it should be possible to evaluate the same CSD from either reflection. However, the authors obtained different power-laws for the same set of samples between the crystallite size (CSD) and the particle size (R_H) with each reflection: $R_H \propto \text{CSD}_{pH}^{1.66}$ from the fit of the 20,11 reflection and $R_H \propto \text{CSD}_{pH}^{3.7}$ from the measurement of the 02,31 FWHM. As shown below, a main reason for this difference is the non-uniqueness of the mathematical solution of the 20,11 fit.

The most common distribution of the crystallite size in a powder sample is by far the lognormal distribution.[4–6] Fig. 1B shows that the lognormal width (ω) modifies the diffraction line profile almost identically to the CSD value, defined here as the mean $\langle D \rangle$ of the ln(CSD) distribution. The $\langle D \rangle$ and ω parameters are so tightly correlated that it is impossible to obtain reliable structural parameters without enforcing some constraints from other knowledge, here the experimental power-law $R_H \propto \text{CSD}_{pH}^{3.7}$. Thus, $\langle D \rangle$ and ω can be estimated iteratively from the 20,11 fit with the constraint that $\langle D \rangle$ matches $R_H \propto [(\langle D \rangle)_{pH}]^{3.7}$ within errors. An example of an invariant XRD profile obtained with five sets of ($\langle D \rangle$, ω) values is shown in Fig. 1C. In practice, the 3.7 exponent can be approached by reducing the [2.8, 7.2] nm CSD interval while refining ω such that $\omega_{pH11} > \omega_{pH8} > \omega_{pH6}$.

Optimizing ($\langle D \rangle$, ω) is supported because the distribution of the crystallite size (ω) in a powder sample depends on the crystal size ($\langle D \rangle$), which itself depends on the conditions of formation.[5] The 2.8 nm size was interpreted

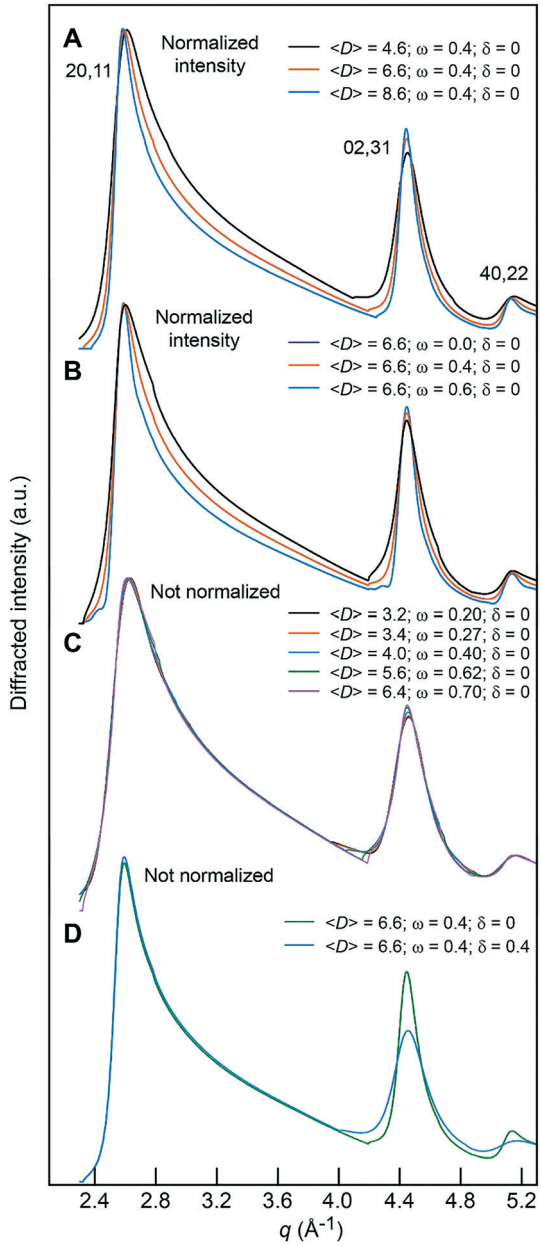

Fig. 1 Effects of the δ-MnO_2 microstructure on the *hk* diffraction line profiles. <*D*> = mean CSD diameter in nm; ω = standard deviation of the lognormal distribution of diameters; δ = strain parameter. A) Effect of the CSD dimension <*D*>. B) Effect of the lognormal width ω. C) Correlation between <*D*> and ω. D) Effect of δ on the intensity and width of the 02,31 reflection. Details on calculations can be found elsewhere.[2] *q* is the scattering vector. *q* (Å^{-1}) = 2π/*d* (Å).

mechanistically in terms of the rapid nucleation and aggregation of δ-MnO_2 crystallites at pH 11 and the 7.2 nm size as the growth of larger nanosheets at pH 3 through the oriented attachment of smaller δ-MnO_2 crystallites. It seems physically realistic that for smaller crystallites, the distribution of size relative to the mean would be larger (*i.e.*, $\omega_{pH11} > \omega_{pH6}$).

The ω parameter is a dimensionless quantity which however gives an indication of the dispersion in the size of the crystallites. A mean CSD diameter <*D*> with a ln(CSD) width ω corresponds to a full-width at half maximum (FWHM) variation (σ_1, σ_2) of

$$(\sigma_1, \sigma_2) = \exp\left[\ln(\langle D\rangle) \pm \sqrt{2\ln(2)}\omega\right]$$

Taking $\langle D\rangle_{pH6}$ = 7.2 nm and ω = 0.5 gives σ_1 = 4.0 nm and σ_2 = 13.0 nm. The same width applied to a $\langle D\rangle_{pH11}$ diameter of 2.8 nm corresponds to a FWHM variation from 1.5 nm to 5.1 nm. Fig. 2 shows that the sensitivity of the lognormal distribution to a heavy tail population of crystallites is increasingly pronounced as the mean (<*D*>) and the dispersion (ω), and hence the asymmetry, of the distribution increase.

Evidence for the non-uniform microstrain deformation of the δ-MnO_2 crystallites

Chemical and biogenic δ-MnO_2 nanosheets are not flat but curled and occasionally kinked.[2,7–13] The bending of the nanosheets causes the crystals to diffract at a higher Bragg angle θ as if they were smaller, because the wavefunctions of the X-rays scattered by atoms at the edges of a crystal go out-of-phase with those at the center. Thus, in principle, the true CSD value can only be determined from the modeling of the 02,31 line using a physically meaningful function of the form

$$\mathrm{CSD}[02,31] = \mathrm{CSD}[20,11] \times f(\theta)$$

A general analytical function is[2]

$$\mathrm{CSD}[hkl]^{-2} = \mathrm{CSD}[\mathrm{real}]^{-2}[1 + \delta(q/q_0)^2]$$

where CSD[real] is the actual size of the crystallite, δ is a dimensionless parameter describing strain, q is the scattering vector, $q = (4\pi/\lambda)\sin\theta$, and q_0 corresponds to the first in-plane reflection. Carrying out the calculation with δ = 0.4 gives CSD[02,31]/CSD[20,11] = 0.68. The strain-broadening effect on the shape of the 02,31 reflection is shown in Fig. 1D. This calculation demonstrates that strain caused the FWHM to

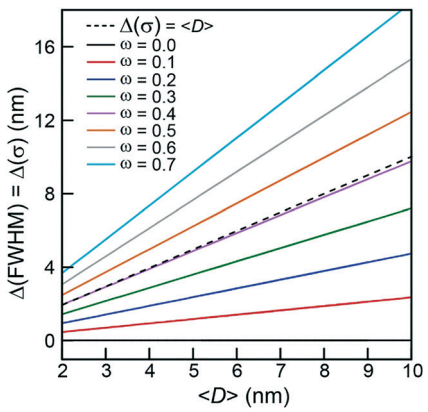

Fig. 2 Variation of the breadth of dispersion of the crystallite size, expressed as Δ(FWHM) = Δσ, with the lognormal mean (<*D*>) and the standard deviation (ω).

broaden by ~65%, and that the peak intensity decreased by the same fraction because the strain does not change the integral breadth of the peak.

Microstrain broadening was observed in all δ-MnO_2 patterns that we have observed (Fig. 3 and ref. 2) and should be general because δ-MnO_2 nanosheets have limited interlayer cohesion and can even be filamentous.[9] Therefore, a provision should be made for this factor in the determination of ($\langle D \rangle$, ω) if it is observed that the intensity ratio of the 20,11 and 02,31 reflections changes between pH 6 and 11.

Together, these considerations call into question how the fits of the *full* XRD patterns ($30° < 2\theta < 75°$) presented in Fig. 2 of Marafatto *et al.*[1] were obtained without considering microstrain effects. An alternative way to match the relative intensities and widths of the 20,11 and 02,31 reflections is to calculate them separately, assuming no microstrain, using different CSD values and normalize arbitrarily their intensities to experiment, as shown in Fig. S1.† This procedure, which embellishes the results, has no physical foundation. It may be necessary to reinvestigate other chemical and biogenic δ-MnO_2 samples[10,14–18] in light of the effects of non-uniform size distribution and strain shown by Manceau *et al.*[2] and the remarks presented here.

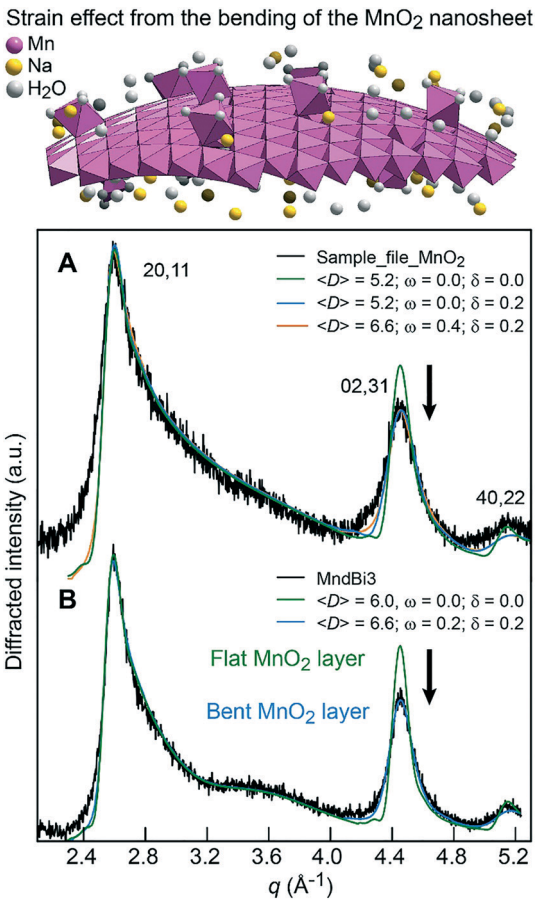

Fig. 3 Experimental and calculated whole-powder patterns for δ-MnO_2 samples showing the contribution of non-uniform strain to the relative intensities of the 20,11 and 02,31 reflections. A) Sample pattern distributed using the current version of the CALCIPOW[19] programme (dated April 2017) maintained by Bruno Lanson.[20] The structural parameters are listed in Table S1.† B) The MndBi3 XRD pattern and structural parameters (except ω and δ) are from Grangeon *et al.*[18]

Conflicts of interest

There are no conflicts to declare.

Notes and references

1 F. F. Marafatto, B. Lanson and J. Peña, *Environ. Sci.: Nano*, 2018, **5**, 497.
2 A. Manceau, M. A. Marcus, S. Grangeon, M. Lanson, B. Lanson, A. C. Gaillot, S. Skanthakumar and L. Soderholm, *J. Appl. Crystallogr.*, 2013, **46**, 193–209.
3 H. Yin, K. D. Kwon, J. Y. Lee, Y. Shen, H. Y. Zhao, X. M. Wang, F. Liu, J. Zhang and X. H. Feng, *Geochim. Cosmochim. Acta*, 2017, **208**, 268–284.
4 V. Drits, J. Srodon and D. D. Eberl, *Clays Clay Miner.*, 1997, **45**, 461–475.
5 J. I. Langford, D. Louër and P. Scardi, *J. Appl. Crystallogr.*, 2000, **33**, 964–974.
6 R. B. Bergmann and A. Bill, *J. Cryst. Growth*, 2008, **310**, 3135–3138.
7 B. M. Tebo, J. R. Bargar, B. G. Clement, G. J. Dick, K. J. Murray, D. Parker, R. Verity and S. M. Webb, *Annu. Rev. Earth Planet. Sci.*, 2004, **32**, 287–328.
8 B. Toner, S. Fakra, M. Villalobos, T. Warwick and G. Sposito, *Appl. Environ. Microbiol.*, 2005, **71**, 1300–1310.
9 N. Miyata, Y. Tani, K. Maruo, H. Tsuno, M. Sakata and K. Iwahori, *Appl. Environ. Microbiol.*, 2006, **72**, 6467–6473.
10 S. Grangeon, A. Manceau, J. Guilhermet, A. C. Gaillot, M. Lanson and L. Lanson, *Geochim. Cosmochim. Acta*, 2012, **85**, 302–313.
11 H. Yin, F. Liu, X. H. Feng, T. D. Hu, L. R. Zheng, G. H. Qiu, L. K. Koopal and W. F. Tan, *Geochim. Cosmochim. Acta*, 2013, **117**, 1–15.
12 H. Yin, X. H. Feng, W. F. Tan, L. K. Koopal, T. D. Hu, M. Q. Zhu and F. Liu, *J. Hazard. Mater.*, 2015, **288**, 80–88.
13 Z. J. Qin, Q. J. Xiang, F. Liu, J. Xiong, L. K. Koopal, L. R. Zheng, M. Ginder-Vogel, M. X. Wang, X. H. Feng, W. F. Tan and H. Yin, *Chem. Geol.*, 2017, **466**, 512–523.
14 M. Villalobos, B. Lanson, A. Manceau, B. Toner and G. Sposito, *Am. Mineral.*, 2006, **91**, 489–502.
15 B. Lanson, M. A. Marcus, S. Fakra, F. Panfili, N. Geoffroy and A. Manceau, *Geochim. Cosmochim. Acta*, 2008, **72**, 2478–2490.
16 S. Grangeon, B. Lanson, M. Lanson and A. Manceau, *Mineral. Mag.*, 2008, **72**, 1197–1209.
17 S. Grangeon, B. Lanson, N. Miyata, Y. Tani and A. Manceau, *Am. Mineral.*, 2010, **95**, 1608–1616.
18 S. Grangeon, B. Lanson and M. Lanson, *Acta Crystallogr., Sect. B: Struct. Sci., Cryst. Eng. Mater.*, 2014, **70**, 828–838.
19 A. Plançon, *J. Appl. Crystallogr.*, 2002, **35**, 377.
20 B. Lanson, http://isterre.fr/bruno-lanson, 2018.